

12

AD-A165 074

## Blowing Model for Turbulent Boundary-Layer Dust Ingestion

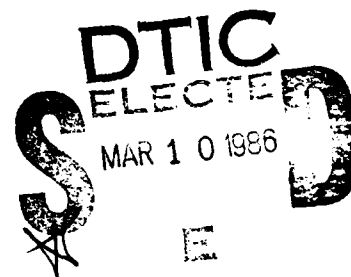
H. MIRELS  
Aerophysics Laboratory  
Laboratory Operations  
The Aerospace Corporation  
El Segundo, CA 90245

10 February 1986

Prepared for  
DEFENSE NUCLEAR AGENCY  
Alexandria, VA 22310

APPROVED FOR PUBLIC RELEASE;  
DISTRIBUTION UNLIMITED

Prepared for  
SPACE DIVISION  
AIR FORCE SYSTEMS COMMAND  
Los Angeles Air Force Station  
P.O. Box 92960, Worldway Postal Center  
Los Angeles, CA 90009-2960



DTIC FILE COPY

86 3 10 058

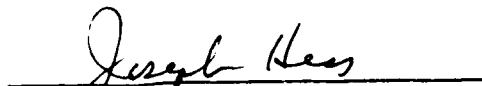
This report was submitted by The Aerospace Corporation, El Segundo, CA 90245, under Contract No. F04701-85-C-0086 with the Space Division, P.O. Box 92960, Worldway Postal Center, Los Angeles, CA 90009-2960. It was reviewed and approved for The Aerospace Corporation by W. P. Thompson, Jr., Director, Aerophysics Laboratory. Capt Charles Thornton, SD/CFP, was the project officer.

This report has been reviewed by the Public Affairs Office (PAS) and is releasable to the National Technical Information Service (NTIS). At NTIS, it will be available to the general public, including foreign nationals.

This technical report has been reviewed and is approved for publication. Publication of this report does not constitute Air Force approval of the report's findings or conclusions. It is published only for the exchange and stimulation of ideas.



CHARLES THORNTON, Capt, USAF  
MOIE Project Officer  
SD/CFP



JOSEPH HESS, GM-15  
Director, AFSTC West Coast Office  
AFSTC/WCO OL-AB

UNCLASSIFIED

SECURITY CLASSIFICATION OF THIS PAGE (When Data Entered)

REPORT DOCUMENTATION PAGE		READ INSTRUCTIONS BEFORE COMPLETING FORM
1. REPORT NUMBER SD-TR-85-97	2. GOVT ACCESSION NO. ADA 165074	3. RECIPIENT'S CATALOG NUMBER
4. TITLE (and Subtitle)  BLOWING MODEL FOR TURBULENT BOUNDARY-LAYER DUST INGESTION		5. TYPE OF REPORT & PERIOD COVERED
7. AUTHOR(s)  Harold Mirels		6. PERFORMING ORG. REPORT NUMBER TR-0086 (6785)-1
9. PERFORMING ORGANIZATION NAME AND ADDRESS The Aerospace Corporation El Segundo, Calif. 90245		8. CONTRACT OR GRANT NUMBER(s)  F04701-85-C-0086
11. CONTROLLING OFFICE NAME AND ADDRESS Defense Nuclear Agency Alexandria, Va. 22310		10. PROGRAM ELEMENT, PROJECT, TASK AREA & WORK UNIT NUMBERS
14. MONITORING AGENCY NAME & ADDRESS (if different from Controlling Office) Space Division Los Angeles Air Force Station Los Angeles, Calif. 90009-2960		12. REPORT DATE 10 February 1986
		13. NUMBER OF PAGES 38
		15. SECURITY CLASS. (of this report)  UNCLASSIFIED
		15a. DECLASSIFICATION/DOWNGRADING SCHEDULE
16. DISTRIBUTION STATEMENT (of this Report)  Approved for public release; distribution unlimited.		
17. DISTRIBUTION STATEMENT (of the abstract entered in Block 20, if different from Report)		
18. SUPPLEMENTARY NOTES		
19. KEY WORDS (Continue on reverse side if necessary and identify by block number) Blowing effects Dust ingestion Dust loading Surface erosion rate Turbulent boundary layer		
20. ABSTRACT (Continue on reverse side if necessary and identify by block number) The rate at which dust is ingested into a turbulent boundary layer is deduced for the case of a semi-infinite flat plate and for the boundary layer behind a moving shock wave. Conventional turbulent boundary-layer theory is used. It is assumed that the local dust-ingestion rate corresponds to the "blowing" rate at which the local unblown surface shear $C_{f,0}$ is reduced to a value $C_{f,t}$ that is just sufficient to maintain surface particles in a mobile state. It is further assumed that the particle-velocity		

DD FORM 1473  
(FACSIMILE)

UNCLASSIFIED

SECURITY CLASSIFICATION OF THIS PAGE (When Data Entered)

UNCLASSIFIED

SECURITY CLASSIFICATION OF THIS PAGE(When Data Entered)

19. KEY WORDS (Continued)

20. ABSTRACT (Continued)

equilibration distance  $l_e$  is small compared with the local boundary-layer thickness  $\delta$ . It is found that erosion rate and boundary-layer thickness parameters are weakly (logarithmically) dependent on  $C_{f,0}/C_{f,t}$  and the maximum dust loading within the boundary layer is approximately equal to one. The theoretical predictions for local erosion rate, boundary thickness, and dust density are compared with the limited experimental results of Hartenbaum and Ausherman for the semi-infinite flat plate and moving-shock cases, respectively. Agreement within about a factor of two is obtained, despite the fact that, for some of the data, the value of  $l_e/\delta$  was of order one. -Further comparison with experiment is recommended.

UNCLASSIFIED

SECURITY CLASSIFICATION OF THIS PAGE(When Data Entered)

## CONTENTS

I.	INTRODUCTION.....	5
II.	THEORY.....	7
	A. Boundary-Layer Equations.....	7
	B. Threshold Shear.....	7
	C. Dust-Ingestion Equations.....	9
	D. Incompressible Flow over a Flat Plate.....	11
	E. Boundary Layer behind a Moving Shock.....	15
	F. Velocity Equilibration.....	18
III.	DISCUSSION.....	21
	A. Flat Plate.....	21
	B. Boundary Layer behind a Moving Shock.....	26
IV.	CONCLUSION.....	33
	REFERENCES.....	35
	APPENDIX: SYMBOLS AND SUBSCRIPTS.....	37

Accession For	
NTIS GRA&I	<input checked="" type="checkbox"/>
DWIC TAB	<input type="checkbox"/>
Unannounced	<input type="checkbox"/>
JUL 1980 Edition	

For [unclear]  
 L [unclear] /  
 [unclear] 7-16-80  
 [unclear] per  
 [unclear]

A-1



## FIGURES

1. Flow Fields and Coordinate Systems for Studying the Ingestion of Dust into a Turbulent Boundary Layer.....	8
2. Variation of Turbulent Boundary-Layer Properties with Variation in $C_{f,0}/C_{f,t}$ for Semi-infinite Flat Plate and Moving-Shock Cases.....	14
3. Experimental Data at $x = 488$ cm for a Turbulent Air Boundary Layer over a Semi-infinite Silica Sand Bed.....	22
4. Experimental Data as a Function of Distance behind a Shock Moving over a Silica Sand Bed.....	27

## TABLES

1. Corresponding Values of Blowing Parameters and Shear Ratio $C_{f,0}/C_{f,t}$ .....	13
2. Comparison with the Hartenbaum <sup>4</sup> Experimental Study of Airflow over a Semi-infinite Sand Bed.....	25
3. Comparison with the Ausherman <sup>5</sup> Experimental Study of a Turbulent Boundary Layer behind a Shock Moving over a Sand Bed.....	32

## I. INTRODUCTION

The interaction of a turbulent wind with a dust-laden surface, and the subsequent lofting of dust particles, is of interest for a variety of applications.

If the surface particles are relatively heavy and the wind speed is not large, the individual particles ejected from the ground rise a certain distance, travel with the wind, and then descend back to the ground. This process, referred to as "saltation," leads to the generation of desert dunes.<sup>1,2</sup> The saltation region occurs in the range<sup>2</sup>

$$0(10^{-2}) < \frac{F_D}{F_g} \equiv \frac{\rho u_\tau^2}{\sigma g d} < 0(1) \quad (1)$$

where  $F_D$  is the aerodynamic drag force on a particle resulting from turbulent fluid motion and  $F_g$  is the gravitational force. Other symbols are defined in the Appendix. The lower limit is related to the minimum force required to loft a particle, and the upper limit corresponds to the limit beyond which the particle goes into suspension. For sand particles in standard air, Eq. (1) becomes approximately  $0(10^4) < u_\tau^2/d < 0(10^6)$ , where  $u_\tau$  (cm/sec) is the local friction velocity<sup>2</sup> (i.e., the characteristic turbulent eddy velocity near a wall) and  $d$  (cm) is particle diameter. For  $d = 10^{-2}$  cm, the friction velocity is limited to values between 10 cm/sec and 100 cm/sec in order for saltation to occur.

With increase in wind velocity, the dust particles enter suspension. This process is of interest in the generation of dust clouds and in the evaluation of nuclear weapons effects.<sup>3</sup> Relatively few experimental studies have been made of dust ingestion into a high-speed turbulent boundary layer. Hartenbaum<sup>4</sup> has investigated air flow over a semi-infinite sand bed with free-stream velocities in the range  $3 \times 10^3$  to  $10^4$  cm/sec and a mean particle diameter  $d = 0.025$  cm. Ausherman<sup>5</sup> has investigated the turbulent boundary layer behind a shock moving over a sand bed with a mean particle diameter  $d = 0.009$  cm. Flow velocities relative to the wall were in the range  $2 \times 10^4$  to  $5 \times 10^4$  cm/sec.

Current analytical models for estimating the local rate of surface erosion generally assume that the erosion rate is proportional to the surface shear that would exist in the absence of lofting (e.g., Refs. 6, 7). The constant of proportionality is deduced from Hartenbaum's experimental results. The dependence of the constant of proportionality on particle and fluid properties is not known. Hence, the range of validity of this approach is uncertain with departure from Hartenbaum's test conditions.

The present study is an attempt to evaluate local erosion rates using conventional turbulent boundary-layer theory. The case considered is one wherein the supply of surface particles is unlimited and the particles reach velocity equilibration with the ambient fluid soon after their injection into the boundary layer. The flow is then similar to the case of a turbulent boundary layer with surface blowing.<sup>8,9,10</sup> It is assumed that the blowing rate is such that the surface shear is reduced to the threshold value of shear at which surface-particle mobility is maintained. A similar approximation was made for the saltation regime in Ref. 2. The theory is described in the next section. Turbulent-layer properties are deduced for a flow of air over a semi-infinite sand bed and for the boundary layer behind a shock moving over a sand bed. Comparisons are made with the experimental observations of Hartenbaum<sup>4</sup> and Ausherman.<sup>5</sup>



## II. THEORY

Integral relations for a turbulent boundary layer, with blowing, are noted. They are solved subject to the assumption that the wall shear equals the threshold value at which surface-particle mobility is maintained. Expressions are derived for the rate of dust ingestion into a turbulent boundary on a flat plate and behind a moving shock wave (e.g., Fig. 1).

### A. BOUNDARY-LAYER EQUATIONS

Consider a turbulent boundary layer with surface blowing and zero pressure gradient. The effect of blowing on local shear and boundary layer thickness can be approximated by

$$\frac{C_f}{C_{f,0}} = \frac{\ln(1 + B)}{B} \quad (1a)$$

and

$$\frac{\delta}{\delta_0} = \frac{1 + B}{B} \ln(1 + B) \quad (1b)$$

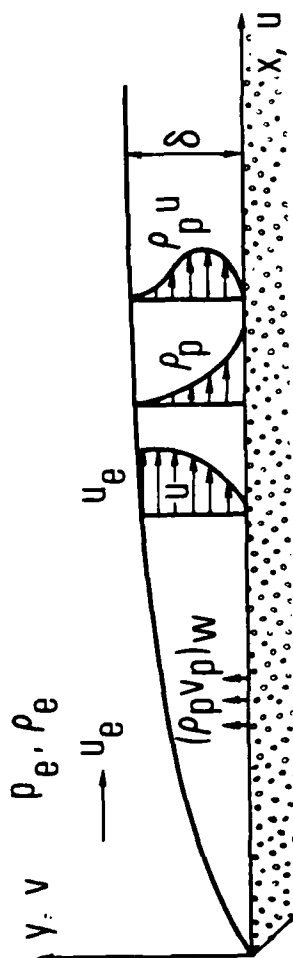
where

$$B \equiv \frac{2}{C_f} \frac{(\rho_p v_p)_w}{\rho_e u_e} \quad (1c)$$

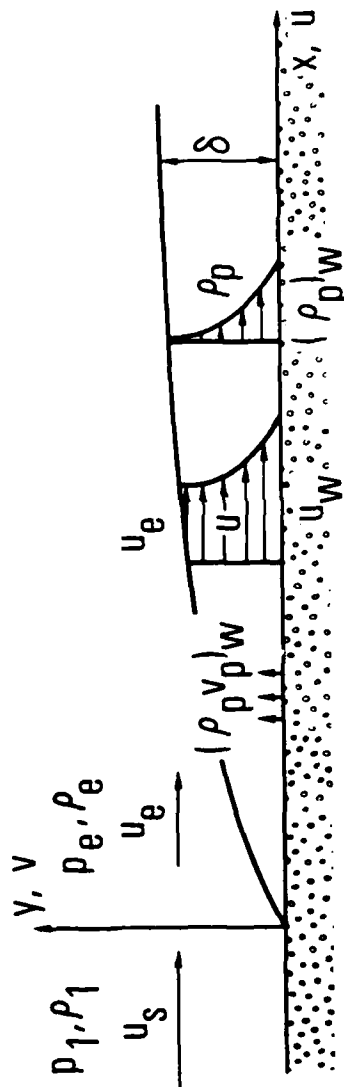
Here subscript zero denotes nonblowing values, and  $(\rho_p v_p)_w$  denotes the local rate at which particles are ingested into the boundary layer. Other symbols are defined in the Appendix. The form of Eq. (1a) can be deduced from a consideration of Couette flow, with blowing,<sup>8</sup> and has been confirmed experimentally<sup>8</sup> for values of the blowing parameter B up to about 20. Equation (1b) is deduced from the momentum integral equation under the assumption that the ratio  $\theta/\delta$  is relatively independent of blowing.<sup>9</sup> Equation (1b) is less well-established than Eq. (1a).

### B. THRESHOLD SHEAR

The lowest value of surface shear at which surface-particle mobility is maintained is termed threshold shear,  $\tau_t$ , and can be expressed by



(a)



(b)

Fig. 1. Flow Fields and Coordinate Systems for Studying the Ingestion of Dust into a Turbulent Boundary Layer. (a) Semi-infinite turbulent boundary layer. (b) Boundary layer behind a moving shock in a shock-stationary coordinate system ( $u_w = u_s$ ).

$$\tau_t = \beta \sigma g d \quad (2a)$$

where  $\beta$  is a dimensionless constant that can be taken equal to <sup>1,2</sup>

$$\beta = 0.0064 \quad (2b)$$

The constant  $\beta$  may be viewed as the ratio of shear force  $\tau_t d^2$  to the gravitational force  $\sigma g d^3$  at which surface-particle motion can be maintained.

### C. DUST-INGESTION EQUATIONS

We now assume turbulent flow over a surface consisting of an unlimited number of small particles. We also assume that the local rate of ingestion of particles into the boundary layer is just sufficient to reduce the local surface shear to the threshold value. Thus,

$$C_f = C_{f,t} \equiv 2\tau_t / \rho_e u_e^2 \quad (3)$$

This assumption is similar to one made in Ref. 2 and assumes, in effect, that small departures of  $C_f$  from  $C_{f,t}$  result in a relatively large blowing rate. Hence, the local blowing rate corresponds to the value needed to reduce the unblown shear  $C_{f,0}$  to a value of order  $C_{f,t}$ . Also, as will be seen,  $B \gg 1$  for cases of practical interest. For these cases the local blowing rate parameter  $(\rho_p v_p)_w / \rho_e u_e$  depends on the log of  $C_f$ . Hence, small departures of  $C_f$  from  $C_{f,t}$  should not significantly affect the result, and Eq. (3) is applicable.

If the surface shear in the absence of blowing  $C_{f,0}$  is known, the local blowing parameter  $B$  can be found from Eqs. (1a) and (3) by iteration, namely

$$B = (C_{f,0}/C_{f,t}) \ln(1 + B) \quad (4a)$$

The local blowing rate is then

$$\frac{(\rho_p v_p)_w}{\rho_e u_e} = \frac{C_{f,t} B}{2} = \frac{C_{f,0}}{2} \ln(1 + B) \quad (4b)$$

and is seen to depend only weakly on  $B$ . Other boundary-layer properties are found as follows. The net particle flux at streamwise station  $x = L$  can be expressed in the alternative forms

$$\dot{M}_p = \int_0^L (\rho_p v_p)_w dx \quad (5a)$$

$$= \int_0^\delta (\rho_p u)_L dy \quad (5b)$$

Equation (5b) assumes velocity equilibration between the particles and the local flow. It will be shown that for the present applications,  $C_{f,0} \sim x^{1/5}$ . If the weak dependence of  $\ln(1+B)$  on  $x$  is ignored, Eq. (5a) becomes

$$\frac{\dot{M}_p}{\rho_e u_e \delta_0} = \frac{5}{8} \frac{x C_{f,0}}{\delta_0} \ln(1+B) \quad (6)$$

where all variables are evaluated at  $x = L$ . In order to evaluate Eq. (5b), we assume

$$\frac{u}{u_e} = 1 - \frac{\rho_p}{(\rho_p)_w} = \left(\frac{y}{\delta}\right)^{1/n} \quad (7)$$

That is, it is assumed that normalized streamwise velocity and particle-density profiles are similar and have a power-law variation with  $y/\delta$ .

Substitution into Eq. (5b) yields

$$\frac{\dot{M}_p}{(\rho_p)_w u_e \delta} = \frac{\theta}{\delta} = \frac{n}{(1+n)(2+n)} \quad (8a)$$

$$= \frac{7}{72} \quad (n = 7) \quad (8b)$$

Equation (8a) is relatively insensitive to  $n$  and the value for  $n = 7$  will be used. Equations (1b), (6) and (8) yield the particle density at the wall, namely,

$$\frac{(\rho_p)_w}{\rho_e} = \frac{45}{7} \frac{x C_{f,0}}{\delta_0} \frac{B}{1+B} \quad (9a)$$

and the particle density profile

The particle velocity at the wall is, from Eqs. (1b), (4b), and (9a)

$$\frac{(v_p)_w}{u_e} = \frac{7}{90} \frac{\delta}{x} \quad (9c)$$

These equations are now evaluated for the case of incompressible flow over a flat plate and for flow behind a moving shock wave.

#### D. INCOMPRESSIBLE FLOW OVER A FLAT PLATE

Consider incompressible flow over a flat plate (Fig. 1a). In the absence of blowing, and ignoring surface roughness effects,<sup>11</sup>

$$\frac{1}{0.0296} \frac{C_{f,0}}{2} = \frac{1}{0.37} \frac{\delta_0}{x} = \left( \frac{\mu_e}{\rho_e u_e x} \right)^{1/5} \quad (10a)$$

Further, consider air at near-standard temperature ( $T_e = 290$  K). The following numerical values then apply:

$$\frac{T_e}{290} \frac{\rho_e}{p_e} = 1.218 \times 10^{-3} \frac{\text{gr}}{\text{cm}^3 \text{ atm}} \quad (11a)$$

$$\left( \frac{290}{T_e} \right)^{1/2} a_e = 3.415 \times 10^4 \frac{\text{cm}}{\text{sec}} \quad (11b)$$

$$\left( \frac{290}{T_e} \right)^\omega \mu_e = 1.829 \times 10^{-4} \frac{\text{gr}}{\text{sec cm}} \quad (11c)$$

where  $\omega = 0.7$ . For sand-like particles

$$\beta = 0.0064 \quad d = 10^{-2} \text{ cm} \quad (11d)$$

$$\sigma = 2.5 \frac{\text{gr}}{\text{cm}^3} \quad g = 980 \frac{\text{cm}}{\text{sec}^2} \quad (11e)$$

The expressions for unblown and threshold shear become

$$\left( \frac{290}{T_e} \right)^{0.24} (M_e p_e x)^{1/5} C_{f,0} = 5.023 \times 10^{-3} \quad (12a)$$

$$\left(\frac{290}{T_e}\right)^{0.24} \left(\frac{M_e p_e x}{M_e^2 p_e}\right)^{1/5} \frac{C_{f,0}}{C_{f,t}} = \frac{2.275 \times 10^4}{\beta d / (6.4 \times 10^{-5})} \quad (12b)$$

where  $p_e$  and  $x$  are in atmospheres and centimeters respectively and the dependence on  $\beta d$  is displayed. Boundary-layer properties are found from

$$\frac{C_{f,0}}{C_{f,t}} = \frac{B}{\ln(1+B)} \quad (13a)$$

$$\left(\frac{290}{T_e}\right)^{0.24} \frac{(M_e p_e x)^{1/5}}{2.511 \times 10^{-3}} \frac{(\rho_p v_p)_w}{\rho_e u_e} = \ln(1+B) \quad (13b)$$

$$\frac{(M_e p_e x)^{1/5}}{3.139 \times 10^{-2}} \frac{\delta}{x} = \frac{1+B}{B} \ln(1+B) \quad (13c)$$

$$\frac{1}{1.03} \frac{(\rho_p v_p)_w}{\rho_e} = \frac{B}{1+B} \quad (13d)$$

These results are applicable for Reynolds numbers beyond the transition value,  $Re_x \gtrsim 10^6$ . Thus, for air, the region of applicability is

$$\left(\frac{290}{T_e}\right)^{1.2} (M_e p_e x) \gtrsim 4.4 \quad (13e)$$

The variation of boundary-layer properties with increase in  $C_{f,0}/C_{f,t}$  is indicated in Table 1 and Fig. 2. For the large values of  $C_{f,0}/C_{f,t}$  of present interest

$$\ln(1+B) \equiv \frac{B}{C_{f,0}/C_{f,t}} = \left(\ln \frac{C_{f,0}}{C_{f,t}}\right) \left\{1 + O\left[\frac{\ln[\ln(C_{f,0}/C_{f,t})]}{\ln(C_{f,0}/C_{f,t})}\right]\right\} \quad (14)$$

Substituting Eq. (14) into Eq. (13) provides an explicit solution for boundary-layer variables in terms of the parameter  $C_{f,0}/C_{f,t}$ . In this region, the local blowing-rate parameter  $(\rho_p v_p)_w / \rho_e u_e$  and the boundary-layer thickness parameter  $\delta/x$  have a weak (logarithmic) dependence on  $C_{f,0}/C_{f,t}$ , as may be

Table 1. Corresponding Values of Blowing Parameters and Shear Ratio  
 $C_{f,0}/C_{f,t}$

$\frac{C_{f,0}}{C_{f,t}}$	B	$\ln(1 + B)$	$\frac{1 + B}{B} \ln(1 + B)$	$\frac{B}{1 + B}$
$1.05 \times 10^0$	$10^{-1}$	$9.53 \times 10^{-2}$	$1.05 \times 10^0$	$9.09 \times 10^{-2}$
$1.44 \times 10^0$	$10^0$	$6.93 \times 10^{-1}$	$1.39 \times 10^0$	$5.00 \times 10^{-1}$
$4.17 \times 10^0$	$10^1$	$2.40 \times 10^0$	$2.64 \times 10^0$	$9.09 \times 10^{-1}$
$2.17 \times 10^1$	$10^2$	$4.62 \times 10^0$	$4.66 \times 10^0$	$9.90 \times 10^{-1}$
$1.45 \times 10^2$	$10^3$	$6.91 \times 10^0$	$6.92 \times 10^0$	$9.99 \times 10^{-1}$
$1.09 \times 10^3$	$10^4$	$9.21 \times 10^0$	$9.21 \times 10^0$	$1.00 \times 10^0$
$8.69 \times 10^3$	$10^5$	$1.15 \times 10^1$	$1.15 \times 10^1$	$1.00 \times 10^0$
$7.24 \times 10^4$	$10^6$	$1.38 \times 10^1$	$1.38 \times 10^1$	$1.00 \times 10^0$

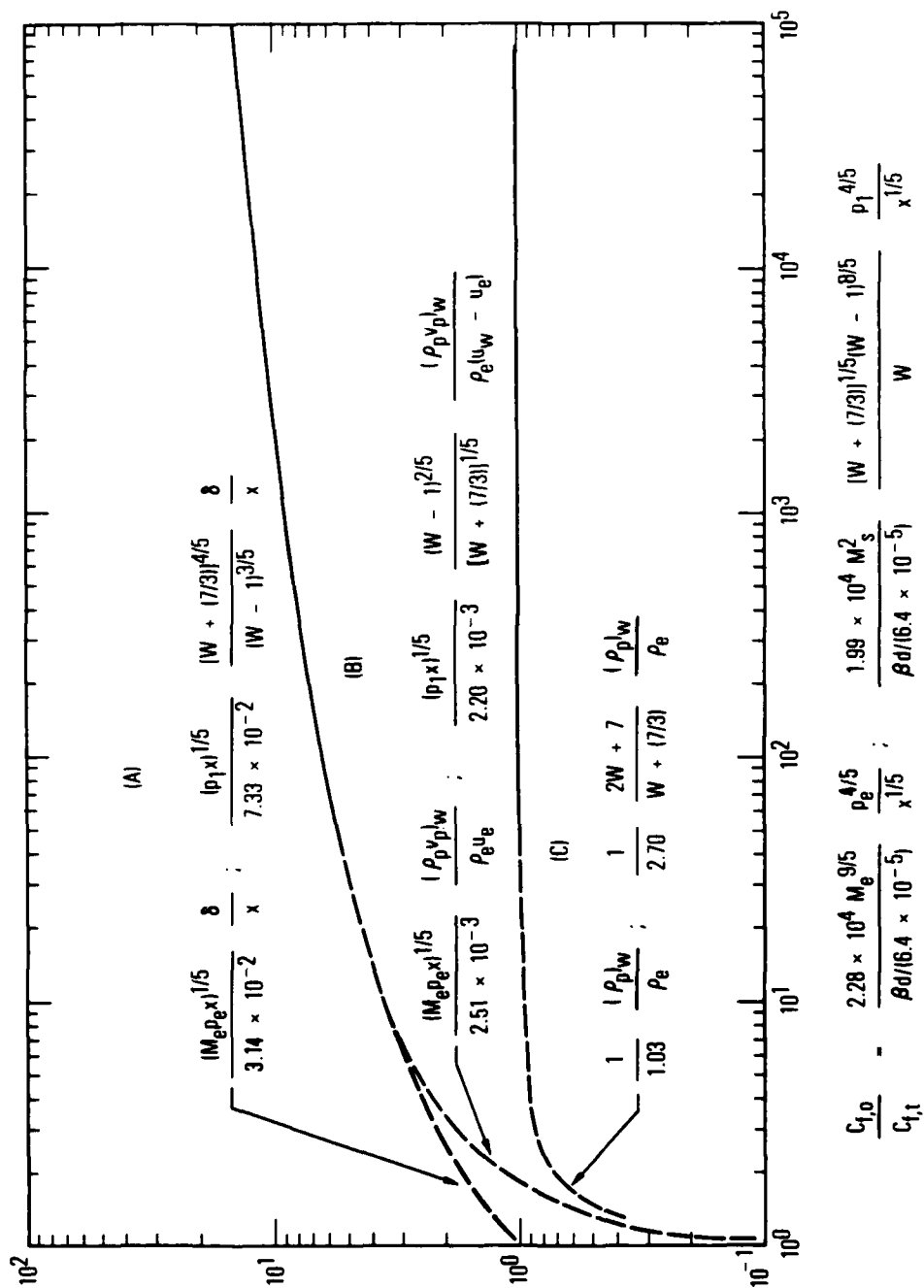


Fig. 2. Variation of Turbulent Boundary-Layer Properties with Variation in  $C_{f,0}/C_{f,t}$  for Semi-Infinite Flat Plate and Moving-Shock Cases. Air,  $T_1 = 290$  K,  $p = \text{atm}$ ,  $x = \text{cm}$ .



observed in Fig. 2. This result is consistent with the previous approximation that the shear can be assumed to be reduced, by blowing, to the threshold value for surface mobility.

For the present case of incompressible flow,  $\rho_w = \rho_e$ . The dust loading at the wall,  $(\rho_p)_w/\rho_w$ , is approximately equal to 1.03 for  $C_{f,0}/C_{f,t} > 10$ . The wall value of dust loading provides an upper bound on the dust loading within the boundary layer. The near-constant value of  $(\rho_p)_w/\rho_w$ , for  $C_{f,0}/C_{f,t} > 10$ , is a reflection of the fact that the blowing rate and boundary-layer thickness grow at the same rate with increase in  $C_{f,0}/C_{f,t}$ .

It has been assumed in the present model that the particles remain in suspension. The saltation layer study by Owen<sup>2</sup> [e.g. Eq. (1)] suggests that this assumption may be invalid when  $C_{f,0}/C_{f,t} < 0$  (100),  $B < 0$  ( $10^3$ ). However, as will be shown, the results of Hartenbaum in Table 2 and Fig. 3a include data at  $C_{f,0}/C_{f,t} = 41.7$  which are consistent with the present model. Hence, the lower limit on  $C_{f,0}/C_{f,t}$ , for which the present results are useful, is not clear. The curves in Fig. 2 are dashed, for  $C_{f,0}/C_{f,t} < 50$ , to reflect the uncertainty in the lower limit of the suspension regime.

#### E. BOUNDARY LAYER BEHIND A MOVING SHOCK

The boundary layer behind a moving shock is illustrated in Fig. 1b. A shock-fixed coordinate system is used. In this coordinate system the wall has a velocity  $u_w$  equal to the upstream flow velocity  $u_s$ . Flow properties upstream and downstream of the shock are denoted by subscripts 1 and e, respectively. Boundary-layer parameters are normalized by the free-stream velocity relative to the wall,  $u_w - u_e$ . Thus

$$C_{f,0} = 2 \tau_{w,0} / [\rho_e (u_w - u_e)^2] \quad (15a)$$

$$C_{f,t} = 2 \tau_t / [\rho_e (u_w - u_e)^2] \quad (15b)$$

$$B = \frac{2}{C_{f,t}} \frac{(\rho_p)_w}{\rho_e (u_w - u_e)} \quad (15c)$$

The normalized velocity and particle-density profiles are

$$\frac{u_w - u}{u_w - u_e} = 1 - \frac{\rho_p}{(\rho_p)_w} = \left(\frac{y}{\delta}\right)^{1/n} \quad (16)$$

The net particle flux at  $x = L$  is [assuming  $C_{f,0} \sim x^{-1/5}$  and neglecting the dependence of  $\ln(1 + B)$  on  $x$ ]

$$\frac{\dot{M}_p}{\rho_e(u_w - u_e)\delta} = \frac{5}{8} \frac{x C_{f,0}}{\delta_0} \frac{B}{1 + B} \quad (17a)$$

or, alternately, for  $n = 7$ ,

$$\frac{\dot{M}_p}{(\rho_p)_w(u_w - u_e)\delta} = \frac{2W + 7}{72(W - 1)} \quad (17b)$$

where  $W = (\rho_e/\rho_1) = u_w/u_e$ . The particle density and velocity at the wall are, respectively,

$$\frac{(\rho_p)_w}{\rho_e} = \frac{5}{8} \frac{72(W - 1)}{2W + 7} \frac{x C_{f,0}}{\delta_0} \frac{B}{1 + B} \quad (18a)$$

and [from Eqs. (1b), (15c), and (18a)]

$$\frac{(v_p)_w}{u_w - u_e} = \frac{4}{5} \frac{2W + 7}{72(W - 1)} \frac{\delta}{x} \quad (18b)$$

In the absence of blowing, the turbulent boundary-layer properties can be expressed (for air with  $T_1 = 290$  K and sand-like particles)

$$(p_1 x)^{1/5} C_{f,0} = 4.397 \times 10^{-3} \frac{[W + (7/3)]^{1/5}}{(W - 1)^{2/5}} \quad (19a)$$

$$\frac{x C_{f,0}}{\delta_0} = 0.0600 \frac{W + (7/3)}{W - 1} \quad (19b)$$

$$\frac{(p_1 x)^{1/5}}{p_1 M_s^2} \frac{C_{f,0}}{C_{f,t}} = \frac{1.991 \times 10^4}{\beta d / (6.4 \times 10^{-5})} \frac{[W + (7/3)]^{1/5} (W - 1)^{8/5}}{W} \quad (19c)$$

The solution, with dust ingestion, is then found from

$$\frac{C_{f,0}}{C_{f,t}} = \frac{B}{\ln(1 + B)} \quad (20a)$$

$$\frac{(p_1 x)^{1/5}}{2.198 \times 10^{-3}} \left( \frac{(W - 1)^2}{W + (7/3)} \right)^{1/5} \frac{(\rho_p v_p)_w}{\rho_e (u_w - u_e)} = \ln(1 + B) \quad (20b)$$

$$\frac{(p_1 x)^{1/5}}{7.328 \times 10^{-2}} \frac{[W + (7/3)]^{4/5}}{(W - 1)^{3/5}} \frac{\delta}{x} = \frac{1 + B}{B} \ln(1 + B) \quad (20c)$$

$$\frac{1}{2.70} \frac{2W + 7}{W + (7/3)} \frac{(\rho_p)_w}{\rho_e} = \frac{B}{1 + B} \quad (20d)$$

In order to insure that the boundary layer is turbulent, we require the equivalent flat-plate Reynolds number<sup>10</sup> to be in the range  $\bar{Re}_x \equiv \rho_e u_e (W - 1)^2 x / \mu_e \geq 10^6$  or, for air,

$$\left(\frac{\mu_1}{\mu_e}\right) \left(\frac{290}{T_1}\right)^{1.2} (M_s p_1 x) (W - 1)^2 \gtrsim 4.4 \quad (21)$$

Equations (20) are identical, in form, with Eqs. (13) and are included in Fig. 2. The weak logarithmic dependence of the blowing rate and boundary-layer thickness parameters on  $C_{f,0}/C_{f,t}$  is again observed. For  $B \rightarrow \infty$  and  $1 < W < 10$ , the particle density at the wall is in the narrow range  $1.00 < (\rho_p)_w/\rho_e < 1.23$ . Evaluation of the dust loading at the wall,  $(\rho_p)_w/\rho_w$ , is more complex than for the previous flat-plate case. If we assume that the wall remains at its initial temperature,  $T_w = T_1$ , ideal gas relations indicate

$$\frac{\rho_w}{\rho_1} = \frac{p_e}{p_1} = \frac{7 M_s^2 - 1}{6} \quad (\text{ideal air}) \quad (22)$$

The dust loading at the wall, for ideal air, is then

$$\frac{(\rho_p)_w}{\rho_w} = 2.70 \frac{W + (7/3)}{2W + 7} \frac{6W}{7 M_s^2 - 1} \frac{B}{1 + B} \quad (23)$$

For strong shocks,  $(\rho_p)_w/\rho_w$  falls below one. This is due to the fact that, for strong shocks, the air density at the wall rises more rapidly with shock strength than does the particle density at the wall. In these cases the peak dust loading  $(\rho_p)/\rho$  occurs within the interior of the boundary layer. However, this feature of the solution may be an artifact of the simplified particle-density profile assumed herein [Eq. (16)].

#### F. VELOCITY EQUILIBRATION

It has been assumed that the particles ingested into the boundary layer rapidly achieve velocity equilibration with the local flow. The region of validity of this assumption is now established.

Assume that the dust particles leave the surface vertically, with a velocity  $v_{p,w}$ . The initial value of drag coefficient is, for spherical

particles,

$$C_{D,p} \equiv \frac{F_D}{[(1/2) \rho_w v_{p,w}^2] [\pi (d/2)^2]} \quad (24a)$$

$$= \frac{24}{Re_d} \quad Re_d \lesssim 10 \quad (24b)$$

$$= 0(1) \quad Re_d \gtrsim 10 \quad (24c)$$

where

$$Re_d = (\rho_w v_{p,w} d) / \mu_w$$

Here  $\rho_w$  and  $\mu_w$  are fluid properties evaluated at the wall [Eq. (24b)] corresponds to Stokes' drag law. Let  $t_E$  denote the time for the particle to reach velocity equilibration with the local fluid. Let  $l_E$  denote the vertical distance from the wall at which velocity equilibration is reached. Approximate values for these quantities are

$$t_E = \frac{l_E}{v_{p,w}} = \left( \frac{v_p}{dv_p/dt} \right)_w \quad (25)$$

where  $(dv_p/dt)_w = F_D/m$ . For spherical particles

$$\frac{x}{d} \frac{l_E}{\delta} = \frac{4}{3} \frac{\sigma}{\rho_w C_{D,p}} \frac{x}{\delta} \quad (26)$$

In the Stokes region,  $Re_d \lesssim 10$ ,

$$\frac{1}{2.02 \times 10^4} \frac{x}{d} \frac{l_E}{\delta} = M_e \phi \quad (\text{plate}) \quad (27a)$$

$$= M_s \frac{2W + 7}{7W} \phi \quad (\text{shock}) \quad (27b)$$

where

$$\phi = \frac{\sigma d}{2.5 \times 10^{-2}} \left( \frac{290}{T_1} \right)^{0.2} \quad (27c)$$

The quantity  $\phi$  equals one for  $T_1 = 290$  K,  $d = 10^{-2}$  cm, and  $\sigma = 2.5$  gr/cm<sup>3</sup>. For  $Re_d \gtrsim 10$ , Eq. (26) is evaluated by assuming  $C_{D,p} = 1$ . In this case,  $\rho_w = \rho_e$  for a flat plate, and  $\rho_w$  is evaluated from Eq. (22) for a moving shock.

The assumption of rapid equilibration is valid when

$$l_E/\delta \ll 1 \quad (28)$$

which can be estimated by using Eqs. (26) and (27). For a given flow, the assumption of equilibration becomes more valid as  $x$  (and therefore  $\delta$ ) increases.

Equation (25) neglects the effect of cross flow on  $l_E/\delta$ . This neglect is valid in the Stokes flow regime but results in an overestimate of  $l_E/\delta$  for  $Re_d \gtrsim 10$  (Ref. 12). The latter estimate is believed adequate for present purposes.

### III. DISCUSSION

Dust ingestion into a turbulent boundary layer on a semi-infinite flat plate and behind a moving shock has been studied experimentally in Refs. 4 and 5, respectively. These experimental results are compared herein with the predictions of the present theory.

#### A. FLAT PLATE

Hartenbaum has reported<sup>4</sup> boundary-layer properties and dust-erosion rates at a distance of  $x = 488$  cm downstream of the leading edge of a silica sand bed. The mean particle diameter was  $d = 0.025$  cm and the test gas was air at standard conditions. Three free-stream velocities ( $M_e = 0.100, 0.212,$  and  $0.336$ ) were considered. His results are indicated in Fig. 3 and Table 2. The predictions of the present theory are included in Table 2 and Fig. 3a.

The local erosion rate was correlated by Hartenbaum in the form (Fig. 3a)

$$(\rho_p v_p)_w = 6.29 \times 10^{-4} u_e^{1.14} \quad (\text{lbm/ft}^2 \text{ sec}) \quad (29a)$$

where  $u_e$  is in ft/sec. For the range of flow conditions in Ref. 4, the present theory gives

$$(\rho_p v_p)_w = 2.70 \times 10^{-4} u_e^{1.12} \quad (\text{lbm/ft}^2 \text{ sec}) \quad (29b)$$

The present theory underestimates the local erosion rate by a factor of 0.4. The exponential dependence on  $u_e$  is remarkably close. It should be noted, however, that Eq. (29b) represents a tangent to the corresponding curve in Fig. 2 and therefore is applicable only for a limited range of  $u_e$  and  $x$ .

Local experimental boundary-layer thickness can be estimated from the velocity profiles in Fig. 3b and is included in Table 2. The predicted boundary-layer thickness is larger than the experimental value by a factor that varies from 2.0 to 1.3 as  $M_e$  increases from 0.100 to 0.336. The experimental value of  $\delta$ , however, is not a well-defined quantity. The edge of

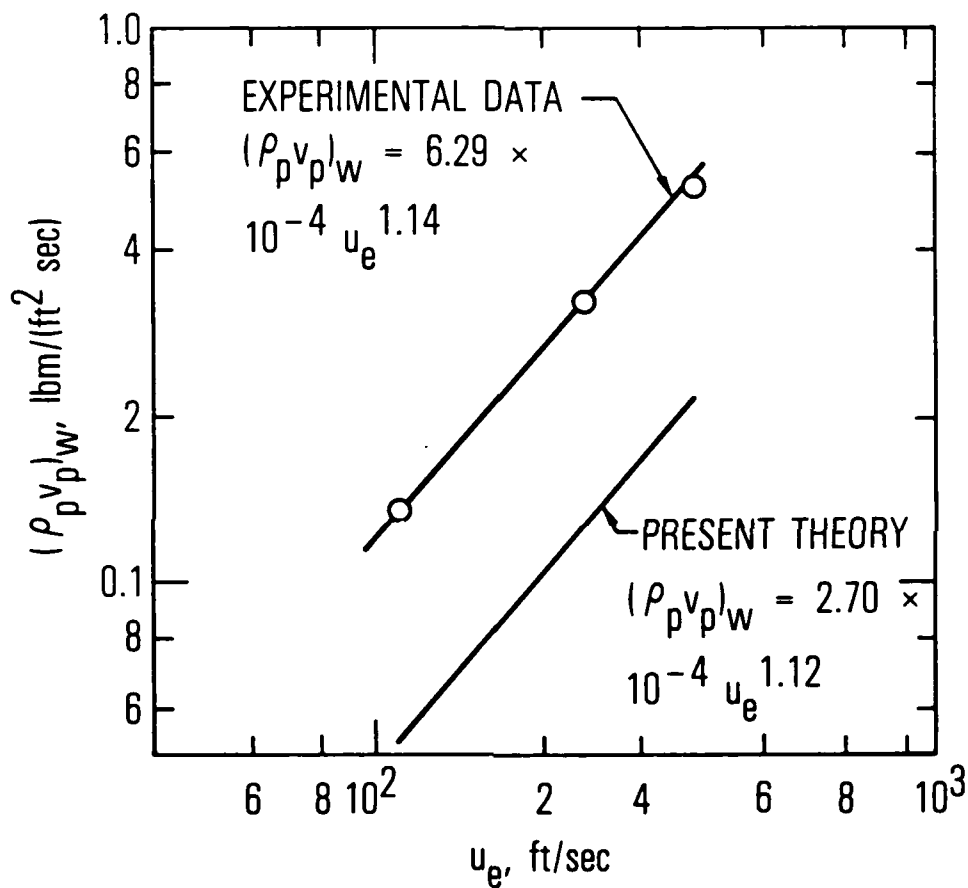
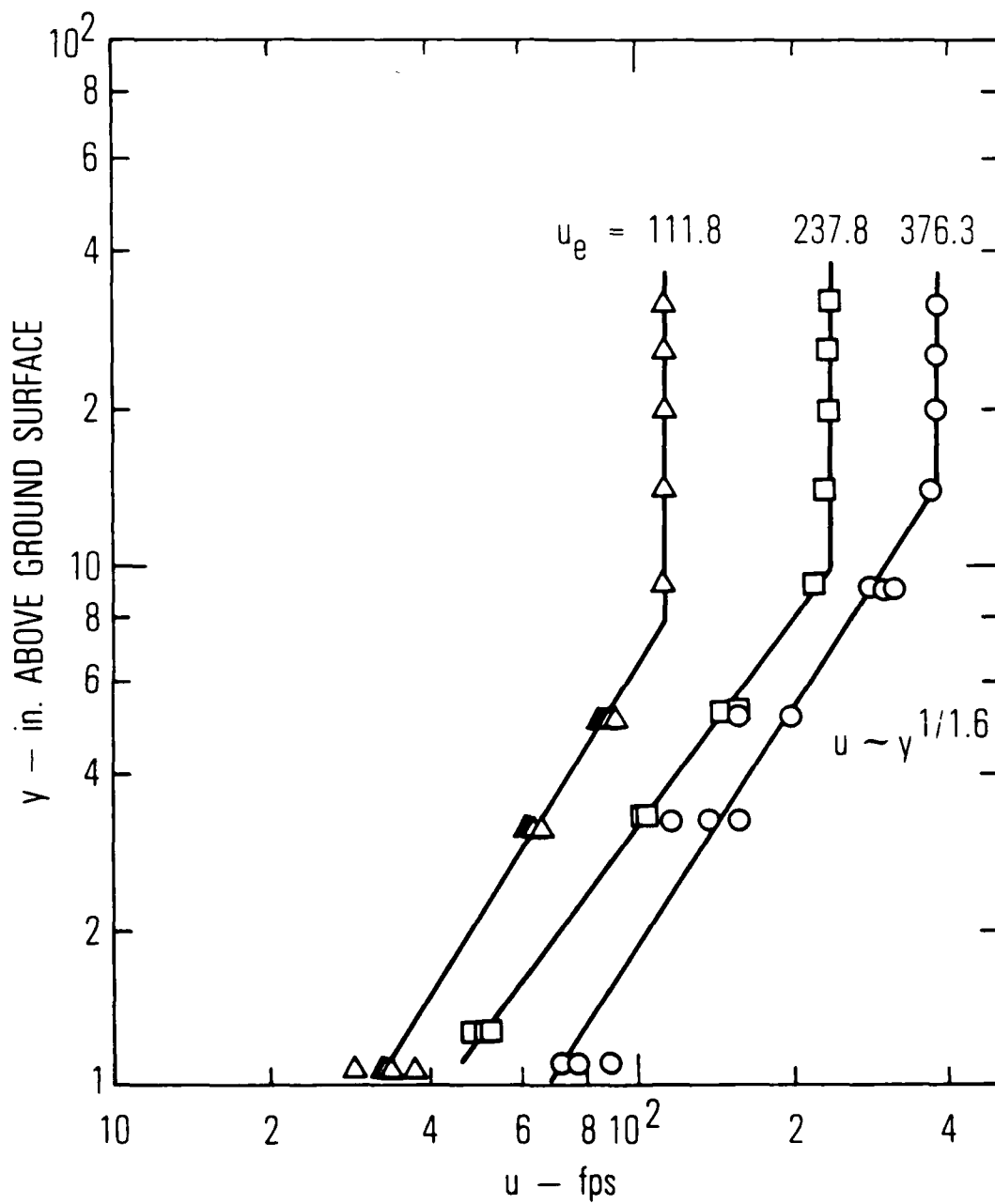


Fig. 3. Experimental Data at  $x = 488$  cm for a Turbulent Air Boundary Layer over a Semi-infinite Silica Sand Bed.  $d = 0.025$  cm,  $p_e = 1$  atm,  $T_e = 290$  K. From Ref. 4. (a) Local mass-erosion rate.





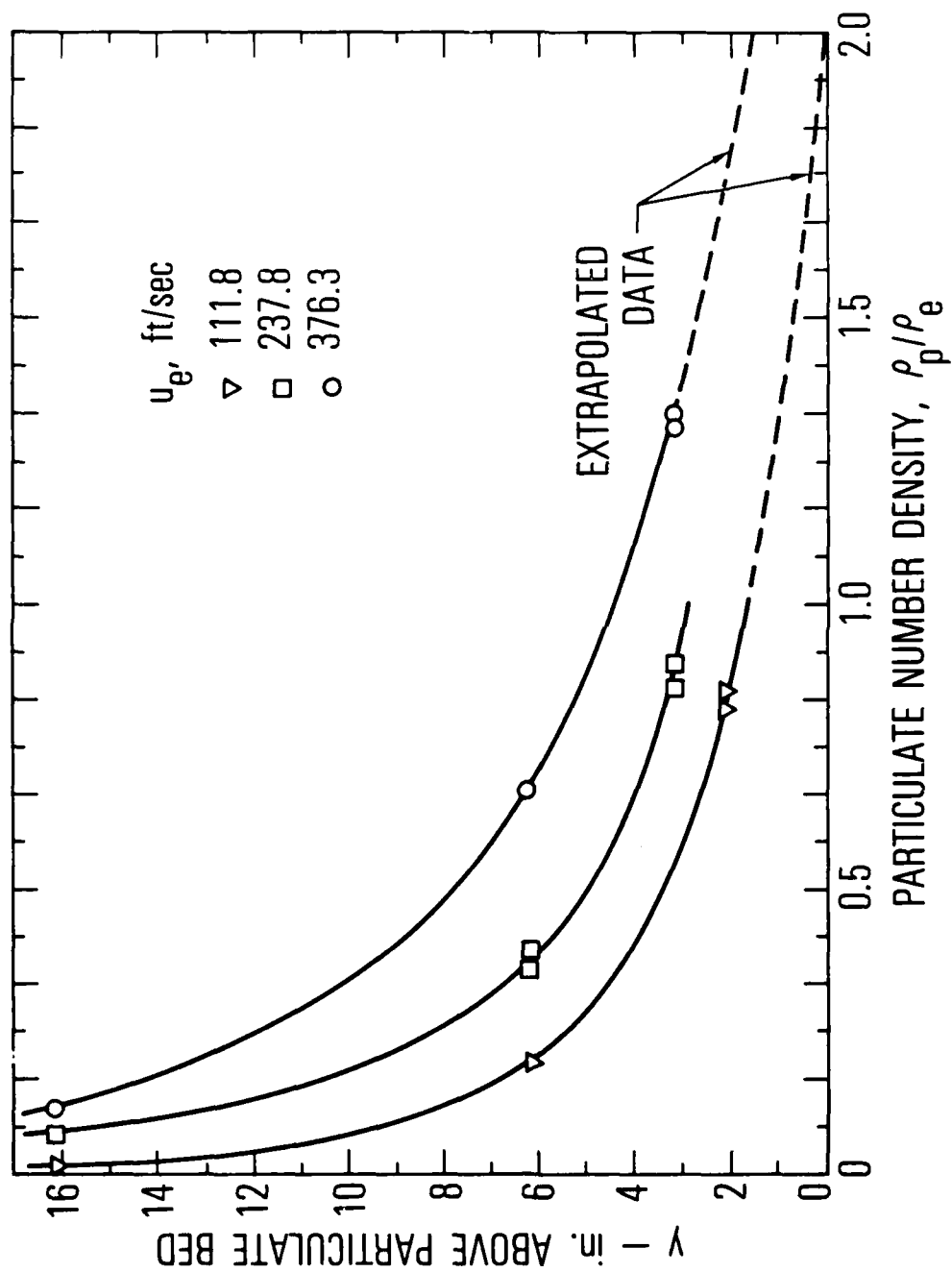


Fig. 3 (Cont'd). (c) Particulate Number-Density Profile,  $\rho_p/\rho_e$ .

Table 2. Comparison with the Hartenbaum<sup>4</sup> Experimental Study of Airflow over a Semi-Infinite Sand Bed. Data taken at  $x = 488$  cm. Ottawa silica sand,  $d = 0.025$  cm,  $T_e = 290$  K,  $P_e = 1$  atm.

$u_e$ , ft/sec	$M_e$	$\frac{C_{f,0}}{C_{f,t}} \times 10^{-1}$	$B \times 10^{-2}$	$Re_d$	Theory			Experiment		
					$\frac{l}{\delta}$	$\frac{\delta}{\delta_0}$	$\frac{\delta}{x} \times 10^2$	$\frac{(\rho)_w}{\rho_e} \times 10^2$	$\frac{(\rho)_w}{\rho_e} \frac{(\rho_v)_w}{\rho_e u_e} \times 10^2$	$\frac{(\rho)_w}{\rho_e} \frac{(\rho_v)_w}{\rho_e u_e} \times 10^2$
111.8	0.0990	4.17	2.26	3.6	0.26	5.45	7.89	1.03	0.626	4.0 ~2 1.6
237.8	0.2123	16.22	11.42	8.4	0.55	7.05	8.78	1.03	0.699	5.0 ~2.5 1.8
376.3	0.3360	37.07	29.64	13.8	0.87	8.00	9.08	1.03	0.724	7.0 ~3 1.9

~ denotes extrapolated value;  $l_e/\delta$  estimated from Eq. (27a)

the dust layer (see Fig. 2c) appears to extend to values of  $y$  which are greater than the experimental values of  $\delta$  inferred from the velocity profiles in Fig. 2b and are in better agreement with present boundary-layer thickness predictions. The experimental velocity profile in Fig. 3b indicates a power law  $u \sim y^{1/n}$  with  $n = 1.6$ , as opposed to the value  $n = 7$  used herein. The reduction in  $n$ , with an increase in blowing rate, is physically realistic. The present theory can be generalized to consider velocity profiles of the form  $y^{1/n}$ , but the extension does not appear warranted at the time.

The dust-density profiles presented in Ref. 4 have been extrapolated to the wall in order to provide a rough estimate of  $(\rho_p)_w/\rho_e$ . Values of 2 to 3 are inferred. These are in approximate agreement with the predicted value of 1.03.

The theoretical estimate for the parameter  $\ell_E/\delta$  increases from 0.3 to 0.9 as  $M_e$  increases from 0.100 to 0.336. Hence the applicability of the theory at the larger values of  $M_e$  may be questioned. However, in view of the fact that no attempt was made to adjust the single free parameter in the present study,  $\beta$ , the agreement between theory and experiment is surprisingly good. The experimental and theoretical predictions of local erosion rate, boundary-layer thickness, and dust density near the wall agree to within about a factor of 2. No systematic divergence between theory and experiment is noted as  $\ell_E/\delta$  increases from 0.3 to 0.8. This suggests that the present theory may be applicable in the extended range  $\ell_E/\delta \lesssim 1.0$ , as defined herein, to within an accuracy of about a factor of 2.

#### B. BOUNDARY LAYER BEHIND A MOVING SHOCK

Ausherman<sup>5</sup> has measured the turbulent boundary layer behind a shock moving over a silica dust bed. The mean particle size was  $d = 0.9 \times 10^{-2}$  cm. Measurements were made at a fixed station, as a function of time after shock arrival, for shocks moving into standard air at  $M_g = 1.41, 1.74$ , and 2.25. Time after shock arrival and distance behind the shock are related by  $t = x/u_g$ . The variation of dust-cloud height with time was evaluated by observing the time at which optical extinction commenced at each of four vertical test positions. The results are given in Fig. 4a. The variation of dust density with height is indicated in Figs. 4b to 4d as a function of time

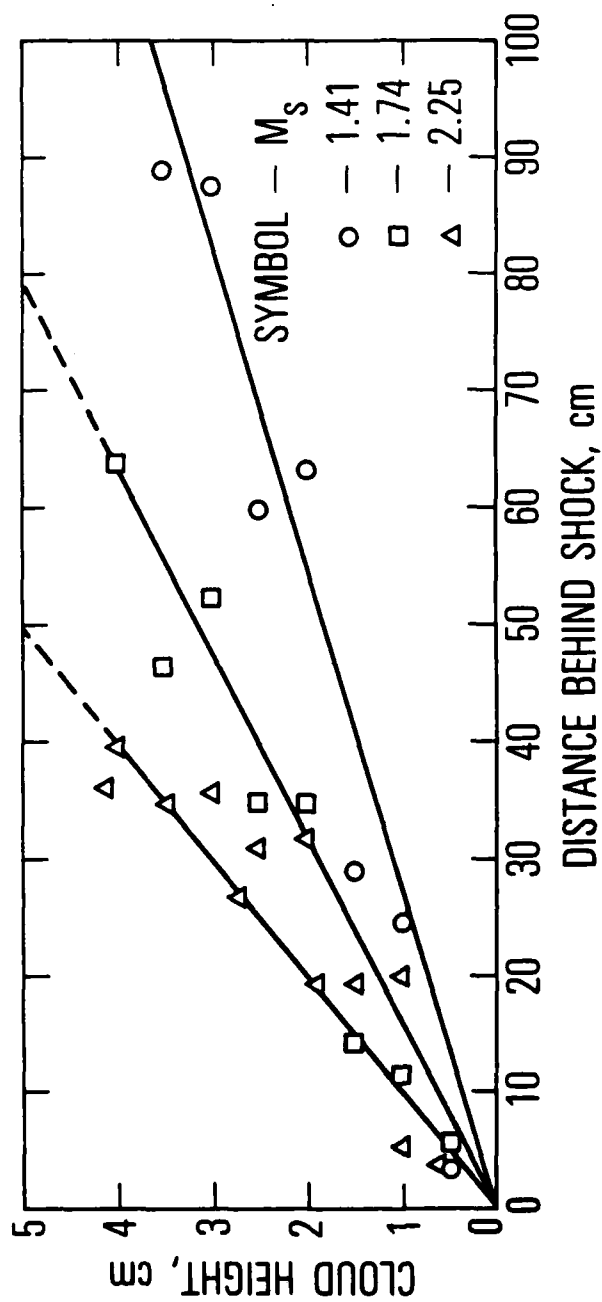


Fig. 4. Experimental Data as a Function of Distance behind a Shock Moving over a Silica Sand Bed.  $d = 0.009$  cm,  $p_1 = 1$  atm,  $T_1 = 290$  K. From Ref. 5. (a) Dust-cloud height vs. distance behind the shock.

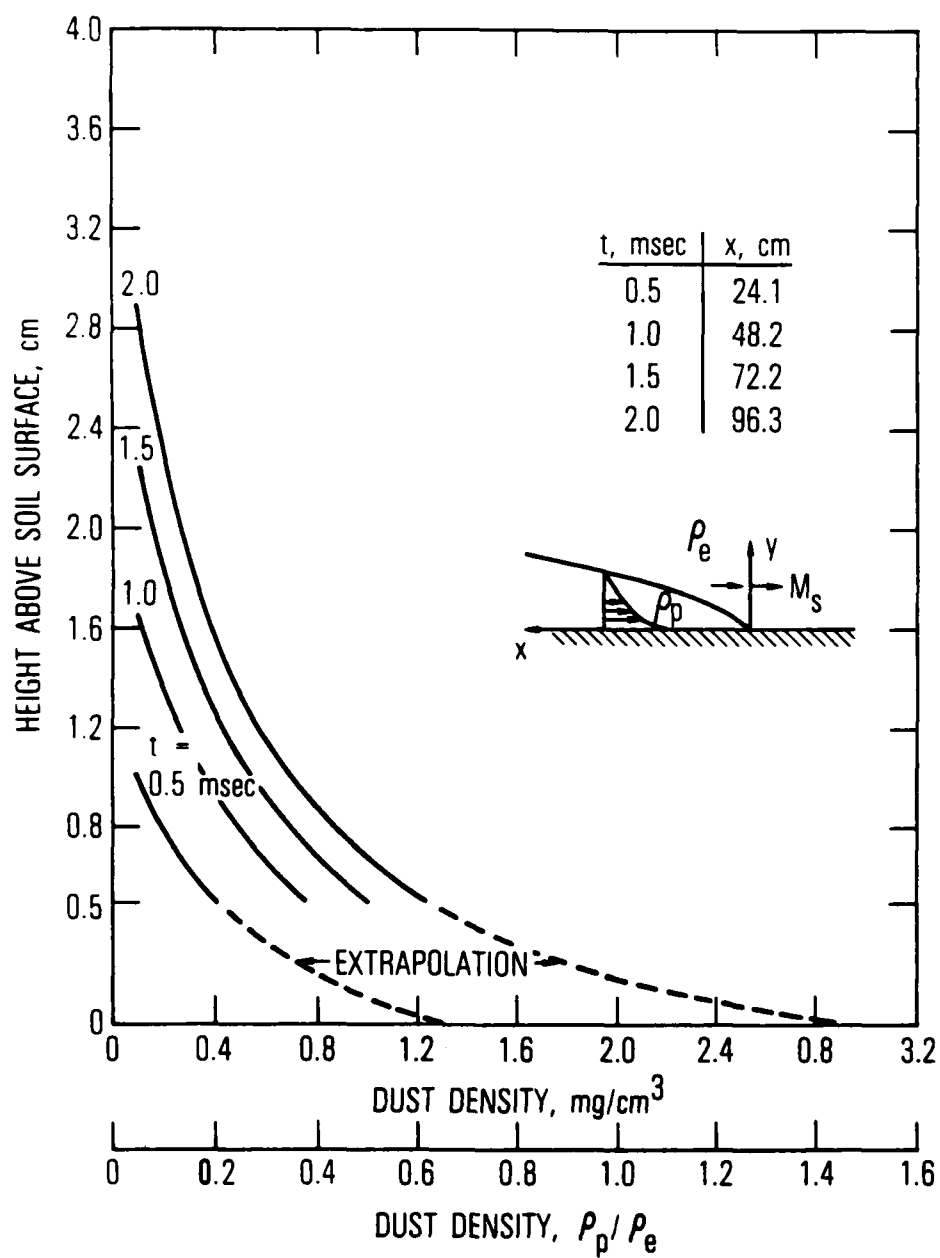


Fig. 4 (Cont'd). (b) Dust-Density Profile ( $M_s = 1.41$ ).

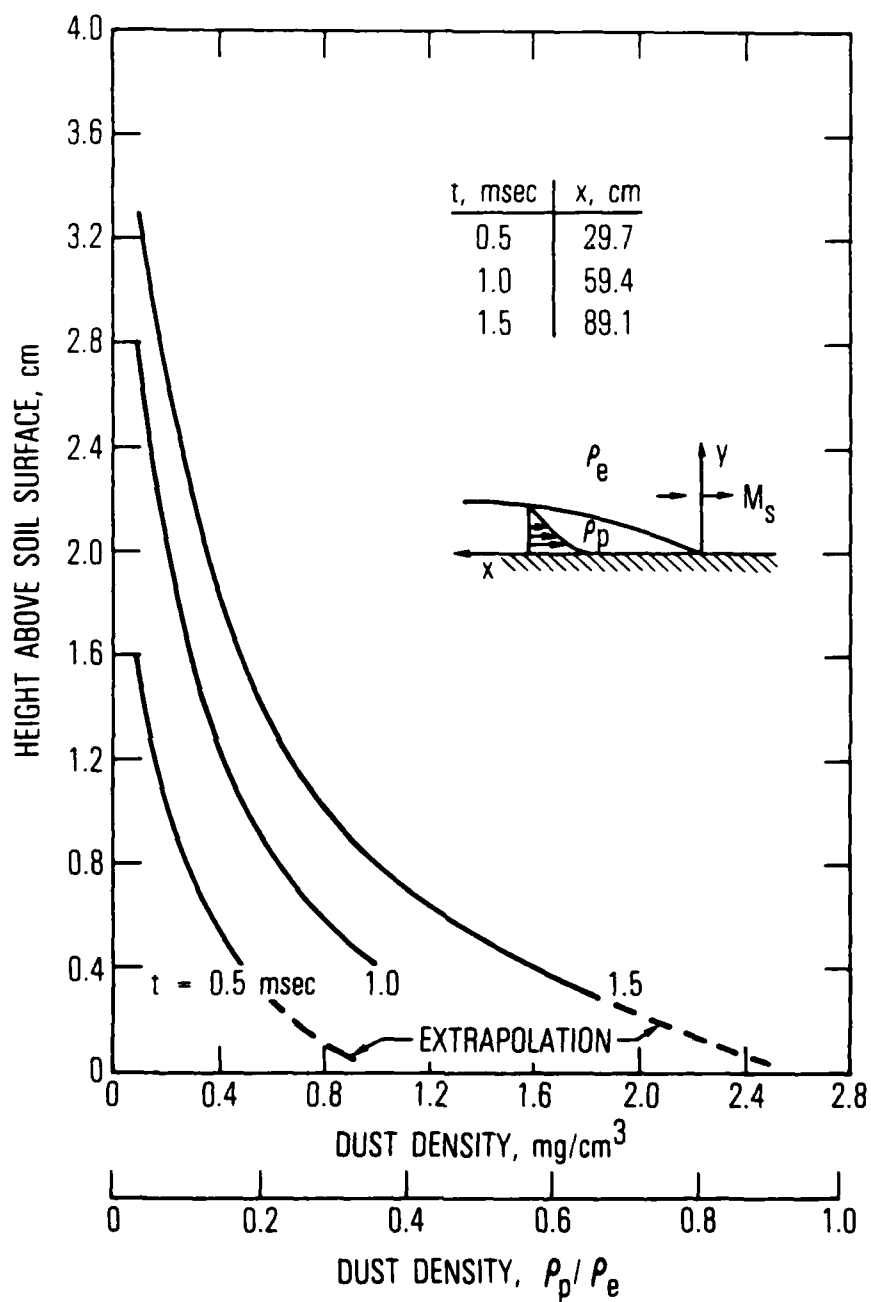


Fig. 4 (Cont'd). (c) Dust-Density Profile ( $M_g = 1.74$ ).

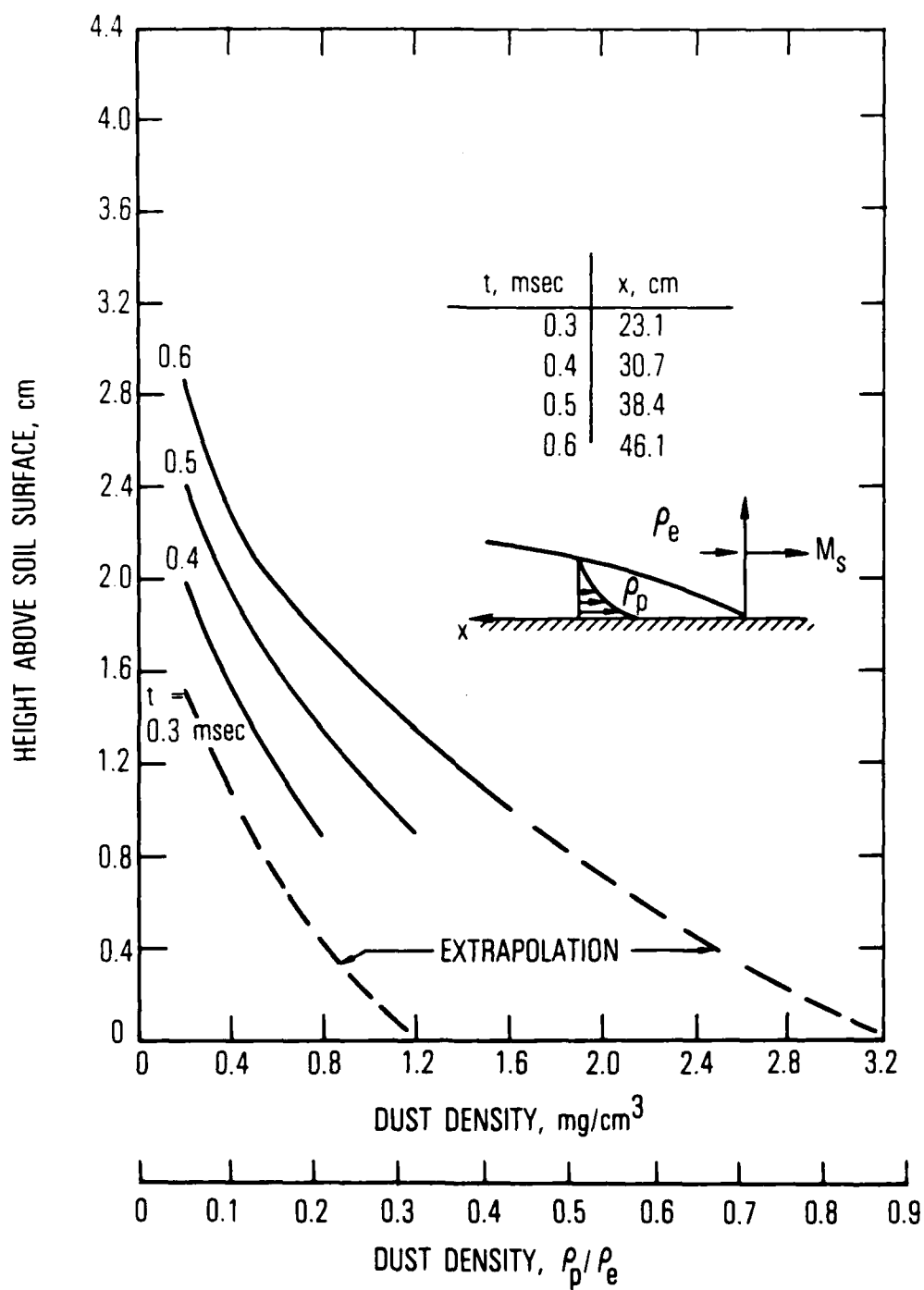


Fig. 4 (Cont'd). (d) Dust-Density Profile ( $M_s = 2.25$ ).



after shock arrival and shock Mach number. The experimental results are compared with theoretical predictions in Table 3.

Comparison of the theoretical and experimental estimates for dust cloud height indicates that the theory overpredicts the height by factors that range from 3.2 to 1.9 for the data in Table 3. The discrepancy is reduced with an increase in  $x$  and  $M_s$ . The magnitude of the overprediction is about the same as for the flat-plate case.

The dust-density profiles were extrapolated to provide estimates of the dust density near the wall. The extrapolated values are in approximate agreement (to within about a factor of 2) with the theoretical predictions.

Values of  $Re_d$  and  $l_E/\delta$  are included in Table 3. The latter has been calculated from Eq. (26) by using  $C_{D,p} = 1$ . It is seen that  $l_E/\delta$  ranges in value from 3.3 to 0.50, with the lower values corresponding to increased  $M_s$  and  $x$ . These values of  $l_E/\delta$ , however, are believed to be overestimates that are due to the neglect of cross flow in the non-Stokes regime.<sup>12</sup> The agreement between theory and experiment appears again to be within about a factor of 2 for those cases where  $l_E/\delta \lesssim 1$ .

Table 3. Comparison with the Ausherman<sup>5</sup> Experimental Study of a Turbulent Boundary Layer behind a Shock Moving over a Sand Bed. Ottawa ultrafine sand,  $d = 0.009$  cm,  $T_1 = 290$  K,  $p_1 = 1$  atm.

$M_0$	$W$	$x$ , cm	Theory						Experiment	
			$\frac{C_{f,0}}{C_{f,t}} \times 10^{-4}$	$B \times 10^{-5}$	$Re_d \times 10^{-1}$	$\frac{l_g}{\delta}$	$\frac{\delta}{x} \times 10$	$\frac{(\rho)_w}{\rho_e} \frac{p_w}{(u_w - u_e)} \times 10^2$	$\frac{(\rho)_w}{\rho_e} \frac{p_w}{x} \times 10$	$\frac{(\rho)_w}{\rho_e}$
1.41	1.71	30.5	1.00	1.16	4.8	3.3	1.15	1.05	1.96	0.36 ~0.8
		61.0	0.87	1.00	4.2	1.9	0.99	1.05	1.69	0.36 ~1.1
		91.4	0.80	0.91	3.8	1.4	0.90	1.05	1.54	0.36 ~1.4
1.74	2.27	30.5	2.97	3.82	10.4	1.5	1.62	1.08	1.76	0.63 ~0.4
		61.0	2.59	3.29	8.9	0.9	1.39	1.08	1.51	0.63 ~0.7
		91.4	2.39	3.01	8.2	0.6	1.28	1.08	1.39	0.63 ~1.0
2.25	3.02	15.2	9.29	13.09	30.2	1.2	2.38	1.11	1.90	1.0 ~0.3
		30.5	8.09	11.27	26.0	0.7	2.05	1.11	1.63	1.0 ~0.6
		45.7	7.46	10.33	23.9	0.5	1.88	1.11	1.50	1.0 ~0.9

~ denotes extrapolated value;  $l_g/\delta$  estimated from Eq. (26) with  $C_{D,p} = 1$

#### IV. CONCLUSION

The present theory contains a number of critical assumptions. The most important are that (1) conventional turbulent boundary-layer correlations apply for very large values of the blowing parameter  $B$ , and that (2) the effect of dust ingestion is to reduce the wall shear to the threshold value needed to maintain surface-particle mobility. In addition, it has been assumed that the local blowing rate is not particle limited and that the particles are in local velocity-equilibration with the ambient fluid. Simple normalized profiles were assumed in order to calculate dust loading.

The theory contains a single free numerical parameter  $\beta$ , which was taken to equal the value recommended by Owen in his study of the saltation process.<sup>2</sup> It is somewhat remarkable that the predicted erosion rates and boundary-layer thicknesses agreed to within about a factor of 2 with the experimental results of Hartenbaum and Ausherman. This agreement may be fortuitous, since the amount of experimental data is meager and some of the data (particularly Ausherman's) violate the assumption  $l_E/\delta \ll 1$ .

A major result of the present study is that for  $C_{f,0}/C_{f,t} \gg 1$ , the boundary-layer parameters have a logarithmic dependence in  $C_{f,0}/C_{f,t}$ , and hence are only weakly dependent on the latter parameter. This should simplify the estimate of local erosion rates in flows of interest. However, further confirmation of the present theory is needed.

# REFERENCES

1. R. A. Bagnold, The Physics of Blown Sands and Desert Dunes (Methuen, London, 1941).
2. P. R. Owen, "Saltation of Uniform Grains in Air," J. Fluid Mech. 20, Part 2, 225-242 (1964).
3. G. W. Ullrich, "Simulation of Dust-Laden Flow Fields," Seventh International Symposium, Military Applications of Blast Simulation, Medicine Hat, Alberta, Canada (13-27 June 1981).
4. B. Hartenbaum, "Lofting of Particulates by a High-Speed Wind," DNA 2737 (September 1971).
5. D. R. Ausherman, "Initial Dust Lofting: Shock-Tube Experiments," DNA 3162F (September 1973).
6. J. W. Kirsch, "Near-Surface Nuclear Dust Cloud Studies," DNA 4332F (January 1977).
7. J. R. Barthel, "Dust Modeling Update" (unpublished), S-Cubed Corporation (December 1982).
8. W. H. Dorrance, Viscous Hypersonic Flow (McGraw-Hill, New York, 1962), pp. 59; 206-220.
9. W. M. Kays and R. J. Moffat, "The Behavior of Transpired Turbulent Boundary Layers," in Studies in Convection, ed. B. E. Launder (Academic Press, New York, 1975), p. 251.
10. H. Mirels, "Estimates of Turbulent Boundary Layer behind a Shock Wave Moving with Uniform Velocity in Air," AIAA-83-0657 (January 1983).
11. H. Schlichting, Boundary Layer Theory (McGraw-Hill, New York, 1960), pp. 16, 485, and 537.
12. G. Rudinger, "Penetration of Particles Injected into a Constant Cross Flow," AIAA Journ. 12, No. 8 (August 1974).

# APPENDIX: SYMBOLS AND SUBSCRIPTS

## Symbols

$a$	speed of sound, cm/sec
$B$	blowing parameter, Eq. (1)
$C_{D,p}$	particle drag coefficient, Eq. (24)
$C_f$	local shear coefficient
$C_{f,0}$	shear coefficient in absence of blowing
$C_{f,t}$	threshold shear coefficient, Eq. (3)
$d$	particle diameter, cm
$F_D$	drag force on particle
$g$	gravitation constant, cm/sec <sup>2</sup>
$L$	streamwise station, cm
$l_E$	particle-velocity equilibration distance, cm
$M$	Mach number, $u/a$
$\dot{M}_p$	net particle flux at station $L$ , Eq. (5)
$m$	particle mass, gr
$n$	velocity profile exponent, Eq. (7)
$n_p$	number of particles per unit volume
$p$	pressure, atm
$Re_d$	particle Reynolds number, $\rho_w v_{p,w} d / \mu_w$
$Re_x$	Reynolds number, $\rho_e u_e x / \mu_e$
$\bar{Re}_x$	equivalent flat-plate Reynolds number, $\rho_e u_e (W - 1)^2 x / \mu_e$
$T$	temperature, Kelvin
$u, v$	fluid velocity in $x, y$ directions

$u_p, v_p$	particle velocity in x,y directions
$u_\tau$	friction velocity, $(2\tau_w \rho_w)^{1/2}$
$W$	density ratio across shock, $\rho_e / \rho_l$
$x, y$	streamwise and vertical direction, cm
$\delta$	boundary-layer thickness
$\theta$	boundary-layer momentum thickness
$\mu$	viscosity, gr/sec cm
$\rho$	fluid density, gr/cm <sup>3</sup>
$\rho_p$	particulate density, n <sub>p</sub> m
$\sigma$	single-particle density, gr/cm <sup>3</sup>
$\tau_w$	surface shear
$w$	viscosity law exponent, Eq. (11)

#### Subscripts

$e$	external to boundary layer
$p$	particle value
$t$	threshold value, Eq. (2)
$w$	surface value
$0$	nonblowing value
$l$	upstream of shock wave

#### LABORATORY OPERATIONS

The Aerospace Corporation functions as an "architect-engineer" for national security projects, specializing in advanced military space systems. Providing research support, the corporation's Laboratory Operations conducts experimental and theoretical investigations that focus on the application of scientific and technical advances to such systems. Vital to the success of these investigations is the technical staff's wide-ranging expertise and its ability to stay current with new developments. This expertise is enhanced by a research program aimed at dealing with the many problems associated with rapidly evolving space systems. Contributing their capabilities to the research effort are these individual laboratories:

Aerophysics Laboratory: Launch vehicle and reentry fluid mechanics, heat transfer and flight dynamics; chemical and electric propulsion, propellant chemistry, chemical dynamics, environmental chemistry, trace detection; spacecraft structural mechanics, contamination, thermal and structural control; high temperature thermomechanics, gas kinetics and radiation; cw and pulsed chemical and excimer laser development including chemical kinetics, spectroscopy, optical resonators, beam control, atmospheric propagation, laser effects and countermeasures.

Chemistry and Physics Laboratory: Atmospheric chemical reactions, atmospheric optics, light scattering, state-specific chemical reactions and radiative signatures of missile plumes, sensor out-of-field-of-view rejection, applied laser spectroscopy, laser chemistry, laser optoelectronics, solar cell physics, battery electrochemistry, space vacuum and radiation effects on materials, lubrication and surface phenomena, thermionic emission, photo-sensitive materials and infrared detectors, atomic frequency standards, and environmental chemistry.

Computer Science Laboratory: Program verification, program translation, performance-sensitive system design, distributed architectures for spaceborne computers, fault-tolerant computer systems, artificial intelligence, microelectronics applications, communication protocols, and computer security.

Electronics Research Laboratory: Microelectronics, solid-state device physics, compound semiconductors, radiation hardening; electro-optics, quantum electronics, solid-state lasers, optical propagation and communications; microwave semiconductor devices, microwave/millimeter wave measurements, diagnostics and radiometry, microwave/millimeter wave thermionic devices; atomic time and frequency standards; antennas, RF systems, electromagnetic propagation phenomena, space communication systems.

Materials Sciences Laboratory: Development of new materials: metals, alloys, ceramics, polymers and their composites, and new forms of carbon; non-destructive evaluation, component failure analysis and reliability; fracture mechanics and stress corrosion; analysis and evaluation of materials at cryogenic and elevated temperatures as well as in space and enemy-induced environments.

Space Sciences Laboratory: Magnetospheric, auroral and cosmic ray physics, wave-particle interactions, magnetospheric plasma waves; atmospheric and ionospheric physics, density and composition of the upper atmosphere, remote sensing using atmospheric radiation; solar physics, infrared astronomy, infrared signature analysis; effects of solar activity, magnetic storms and nuclear explosions on the earth's atmosphere, ionosphere and magnetosphere; effects of electromagnetic and particulate radiations on space systems; space instrumentation.